Dealloyed Pt−Cu Core−Shell Nanoparticle Electrocatalysts for Use in PEM Fuel Cell Cathodes

Prasanna Mani, Ratndeep Srivastava, and Peter Strasser*

Department of Chemical & Biomolecular Engineering, University of Houston, 4800 Calhoun Road, Houston, Texas 77004

Received: September 22, 2007; In Final Form: November 17, 2007

We report the synthesis, characterization, and single fuel cell testing of a novel class of nanostructured Pt−Cu alloy particle materials for use as oxygen reduction electrocatalyst in polymer electrolyte membrane fuel cells. The active phase of the Pt alloy nanoparticle catalysts is prepared by electrochemical dissolution (voltammetric dealloying) of Cu surface atoms from Cu-rich Pt−Cu alloy precursors. Bulk and surface structural and compositional characterization suggests that the dealloyed active catalyst phase consists of a core−shell structure in which a multilayer Pt rich shell is surrounding a Pt-poor alloy particle core. The electrocatalytic Pt mass activity of the dealloyed core−shell particles for the oxygen reduction reaction (ORR) exceeds that of state-of-the art Pt electrocatalyst by more than a factor of 4 and thus meets performance targets for fuel cell cathodes [Gasteiger, H. A.; Kocha, S. S.; Sompalli, B.; Wagner, F. T. *Appl. Catal. B: Environ.* **2005**, *56*, 9−35].[1] It is hypothesized that a reduced Pt−Pt distance near the particle surface, stabilized by the lattice-contracted alloy core, may explain the modification of the surface catalytic reactivity. Dealloying of base-metal-rich noble metal alloy precursors is proposed as a more general strategy toward modifying the surface catalytic properties of noble metal surfaces.

1. Introduction

Our planet's well-being is increasingly linked to the availability of clean, secure, and sustainable energy. To reduce our dependence on oil as the primary transportation fuel source, to realize energy efficiency improvements, and to address environmental concerns associated with the use of fossil energy carriers, a large amount of research is currently being performed on new materials and enabling technologies for producing, storing, and using hydrogen as a renewable energy carrier. Due to their high theoretical efficiency,[2,3] polymer electrolyte membrane fuel cells (PEMFCs) will play a critical role as power sources in a hydrogen-based energy infrastructure. The heart of a PEMFC is a 3-layer membrane electrode assembly (MEA), consisting of anode, membrane electrolyte, and cathode, where hydrogen and oxygen are catalytically converted into water and electricity. The operating conditions and performance characteristics of PEMFCs make them currently the most attractive fuel cell technology for use in automotive and stationary applications.[4]

Currently, PEMFCs continue to face severe performance and durability challenges associated with their materials and components. Paramount among them is the performance of the cathode electrocatalyst where molecular oxygen and protons are converted to water in the oxygen reduction reaction (ORR). Unsupported or carbon-supported pure Pt materials have been the most widely used cathode electrocatalysts for decades.

Pt−Co alloys have been studied extensively for use as ORR electrocatalysts in fuel cells[5−10] and have been consistently found to offer an intrinsic enhancement of the electrocatalytic ORR activity on a Pt mass and surface-area basis. More than two decades ago, United Technologies Corporation (UTC) and others reported on the use of Pt−Co alloys for ORR in phosphoric acid fuel cells (PAFCs)[5,11]. Early reports on the use of Pt−Co alloys for ORR in polymer electrolyte membrane fuel cells (PEMFCs) were authored by Mukerjee et al.[7] Pt mass based activity enhancements of Pt−Co alloys of a factor of 1.5−2.5 compared to pure Pt have repeatedly been reported.[8,10,13−25]

Its performance is generally expressed as the ratio between the catalytic oxygen reduction activity (cell current at given cell potential) and the cost (equivalent to the employed mass) of the platinum electrocatalysts at the PEMFC cathode. This ratio is generally referred to as the cathode Pt mass activity.[1] It has been estimated that the cathode Pt mass activity has to be improved by a factor of at least 4 compared to ∼45 wt % Pt/C standard catalyst before automotive PEMFC cost targets can be met.[1] On a molecular level, the performance limitations of a PEMFC are mainly caused by the sluggish kinetics of the electroreduction of molecular oxygen to water at the cathode,[24,25] which is believed to be a result of a fairly strong Pt−O surface bond.[24] The search for more active ORR electrocatalysts with reduced Pt content is progressing in two directions; one is focusing on Pt alloys[25−28] and the other investigates non-Pt catalyst concepts.[1,29]

Among Pt alloys, three distinct catalyst concepts have received attention: First, Pt-rich Pt−Co catalysts[1,10] have been showing much promise in terms of Pt-mass-based performance improvements. Their Pt-mass-based fuel cell activities showed an improvement of about 2−3× compared to pure Pt. Second, Pd-supported Pt monolayer electrocatalysts were reported to exhibit double-digit Pt-mass based activity gains.[30] But taking Pd into consideration, their noble-metal-mass activity gains dropped to 2−3×. Finally, a $Pt_3Ni(111)$ single-crystal surface exhibited extraordinary double-digit Pt-mass activity improvements compared to pure Pt.[27] The activity increases of the latter two catalyst concepts were demonstrated in electrochemical half-

* Corresponding author. Phone: +1 (713) 743 4310. Fax: +1 (713) 743 4323. E-mail: pstrasser@uh.edu.

10.1021/jp0776412 CCC: $40.75
Published on Web 01/26/2008

cell experiments and liquid electrolytes. Their realization in real MEAs remains challenging. In contrast, Pt−Co catalysts have been implemented and a 2−3× activity improvement has been realized in real single PEMFCs.[1]

In this article we report on a novel class of highly active, surface de-alloyed Pt−Cu nanoparticle electrocatalysts for the electro-reduction of oxygen at PEMFC cathodes. In a previous report we demonstrated in rotating disk electrode experiments[31] how surface dealloying can be used as an effective strategy to modify the surface electrocatalytic properties of noble metal alloys. Here, we extend this work to MEA testings and critically compare the effectiveness of chemical (acid wash) versus electrochemical dealloying strategies, demonstrate how the active catalyst phase can be prepared in situ by electrochemical dealloying inside the cathode layer of MEAs, realize a Pt-mass activity improvement of a factor of 4 times in single PEMFCs and characterize the electrocatalysts structurally and compositionally before and after electrocatalysis.

2. Experimental Methods

2.1. Catalyst Synthesis and Characterization. Pt−Cu alloy precursors were prepared by an impregnation/freeze drying route followed by annealing. Preparation started with impregnation and sonication of a commercial 30 wt % Pt/C catalyst (Tanaka Kikinzoku International, Inc.) with an aqueous solution of a copper nitrate (Sigma-Aldrich, Inc.), followed by freezing in liquid N_2. The frozen sample is subsequently freeze-dried under a moderate vacuum (0.055 mbar). Reduction and alloying of Pt and Cu on the carbon support was thermally driven under a reductive H_2 atmosphere using a Lindberg/Blue tube furnace. The bulk atomic composition of the catalysts was determined using a JEOL JSM6330F energy dispersive spectrometer (EDS) after calibrating with the respective pure metal standards or using a VARIAN 820-MS inductively coupled plasma-mass spectrometer (ICP−MS) after blank and standard measurements. Surface atomic composition of the nanoparticles was performed by PHI Model 5700 X-ray photoelectron spectrometer (XPS).

2.2. MEA Fabrication and Dealloying Procedure. Catalyst pastes were prepared by initially blending about 0.13 g of wetted (few drops of deionized water) carbon-supported Pt or Pt−Cu alloy catalyst with 42 mL of refrigerated (15 min) isopropyl alcohol (Aldrich, HPLC grade), followed by 15 min stirring and ultrasonication (Branson 150) for 1 h. Thereafter, about 0.83 grams of a 5 wt % Nafion solution was added until a catalyst : Nafion dry weight ratio of about 3:1 was obtained, followed by additional sonication for 1 h. For the anode layer a commercial 40 wt % Pt/C (E-tek Inc.) was used. MEAs were prepared by spraying these pastes through an atomizing nozzle directly onto the Nafion NRE212 membrane using a high-precision robotic machine (PVA Inc.), followed by heat treatment at 80 °C.

Pt−Cu precursor was dealloyed either by a chemical or an electrochemical method. In chemical dealloying, the precursor powders were treated with 1 M H_2SO_4 at 80 °C for 36 h and then washed several times with deionized water. Finally the Cu-ion-free catalyst was frozen in liquid N_2 and vacuum-dried over night. The dealloyed catalyst powder was then used to prepare the cathode layer. In electrochemical dealloying, the precursor material was used to prepare the catalyst paste which was applied as the cathode layer of an MEA.

The MEA was assembled with fuel cell components (see section 2.3 below) and hydrated at 80 °C, 100% RH (H_2/O_2), 101.3 $kPa_{(abs)}$ by holding cell potential at 0.6V for 4 h. Then the cathode potential was cycled 200 times at 100mV/s between 0.5−1.0 V /RHE in de-oxygenated condition at 80 °C, 100% RH (H_2/N_2), 101.3 $kPa_{(abs)}$ to electrochemically dealloy the cathode catalyst. The MEA was then disassembled and treated twice with liquid 1 M H_2SO_4 at 80 °C for 1 h each. Between and after ion exchange washings the MEA was rinsed with deionized water. The single cell was then re-assembled with fresh gas diffusion media for fuel cell testing of the dealloyed catalyst. During the break-in procedure (before constant potential activation, after dealloying, and after ion exchange) slow 20 mV/s CVs were recorded between 0.05−1.2 V in order to characterize the electrochemical interface and the extent of the Cu dealloying.

2.3. Fuel Cell Testing. The prepared MEAs with active area of 10 cm^2 were then assembled with gas diffusion media [GDL 10BC (Sigracet, SGL Carbon Inc.)], 3-channel serpentine flow fields (Poco graphite blocks) and gold-coated current collectors and tested in a fuel cell station supplied by Fuel Cell Technologies Inc. The relative humidities of the feed streams for anode/cathode were set at 100% at 80 °C cell temperature. The MEAs were activated with a break-in protocol under 150 kPa_{abs} pressure before recording current−voltage characteristics, also 150 kPa_{abs}. Polarization curves were taken using flows of stoichiometry flows of $\lambda = 2/10$ (H_2/O_2) for $i \geq 0.2$ and 0.2 A/cm^2 flows for $i < 0.2$ A/cm^2. The performance of the fuel cell was monitored by a data acquisition system from start to stop. IR correction was done by correcting the cell voltage with measured ohmic resistance of the fuel cell by an inbuilt AC impedance analyzer operating at 1 kHz frequency.

2.4. Electrochemical Characterization. To accurately measure the activation polarization of the catalyst, it is essential to determine the H_2 crossover current in the fuel cell determined by linear sweep voltammetry (LSV). This is done by sweeping the potential at 5 mV/s from 0.05 to 0.6 V (at the same temperature) after $i-V$ recording. At >0.4 V the resulting hydrogen oxidation current is purely limited by the H_2 permeation rate. Cyclic voltammetry (CV) was performed to dealloy the Cu rich Pt−Cu precursor cathodes (0.5−1.0 V, 80 °C cell temperature, 100% RH of H_2/N_2) and to measure the electrochemical surface area ($ECSA_{Pt}$) of Pt/C and Pt−Cu/C catalysts (0.05−1.2 V, 30 °C cell temperature, 50 °C dew point of H_2/N_2 to ensure complete hydration of the electrolyte and to obtain maximum $ECSA_{Pt}$). The scan rate to record the voltammogram was 100 mV/s for dealloying and 20 mV/s for measuring $ECSA_{Pt}$ and the charge for monolayer hydrogen adsorption/desorption was assumed to be 210 $\mu C/cm^2_{Pt}$. For CV or LSV, the H_2 anode served as a counter and reference electrode and the N_2-purged cathode was the working electrode, with gas flow of $H_2/N_2 = 170$ mL/min. All of the voltages here are reported vs the reversible hydrogen electrode (RHE).

3. Results and Discussion

3.1. Concept and Preparation of Voltammetric Dealloyed Bimetallic Nanoparticle Catalysts. Figure 1 illustrates the synthetic strategy and the structural characteristics of the active catalyst phase of surface dealloyed Pt bimetallic alloy nanoparticles. A Cu-rich $Pt_{25}Cu_{75}$ bimetallic alloy nanoparticle precursor is applied as ORR electrocatalyst in the cathode layer of an MEA (Figure 1a) and, after complete cell assembly, is subjected to voltammetric cycling between 0.5 and 1.0 V/RHE. Owing to the large difference in electrochemical corrosion potential, Cu ions are selectively removed from the precursor particles and remain trapped at the negatively charged SO_3^- groups of the Nafion polymer inside the electrode layer and inside the MEA membrane (Figure 1b). The selective electro-

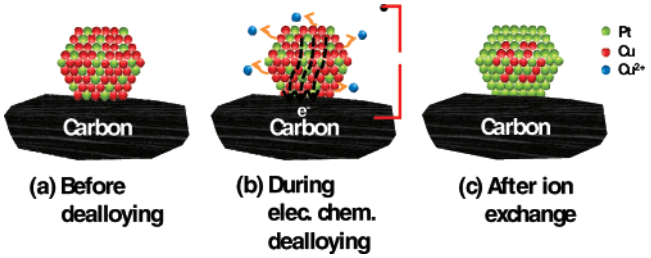

Figure 1. Illustration of the stepwise in-situ preparation of dealloyed Pt−Cu electrocatalysts by voltammetric selective dissolution of Cu from a $Pt_{25}Cu_{75}$ precursor catalyst. (a) Carbon supported $Pt_{25}Cu_{75}$ precursor at a MEA cathode. (b) Electrochemical dissolution of Cu atoms from precursor by cyclic voltammetry. (c) Formation of a Pt enriched core−shell nanoparticle catalyst with surrounding Cu ions removed by ion exchange.

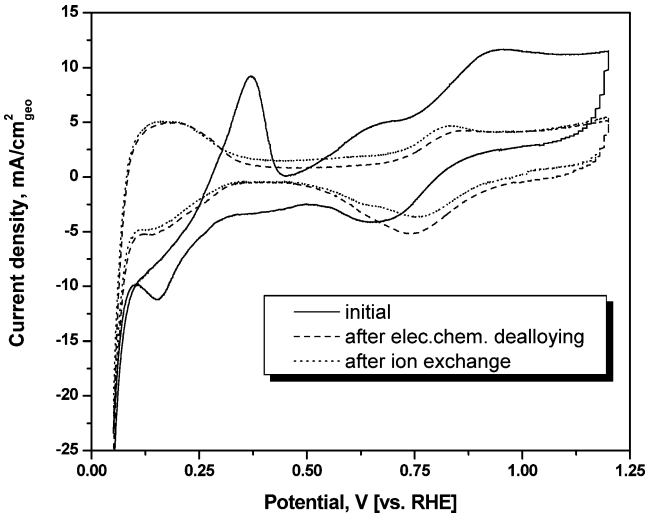

Figure 2. Cyclic voltammograms of a $Pt_{25}Cu_{75}$ fuel cell cathode catalyst recorded at three different stages during the in-situ preparation of dealloyed of Pt−Cu nanoparticle catalysts (compare Figure 1). Scan rate 20 mV/s. Anode: H_2; Cathode: N_2, 10 cm^2 active area, 100% RH, total pressure 101.3 kPa.

chemical dissolution of Cu (voltammetric Cu dealloying) results, as will be shown in this section, in a dealloyed nanoparticle with a Pt-enriched near surface region surrounding a Cu-rich alloy core (core−shell structure). Finally, the MEA is disassembled from the single cell and immersed in hot liquid acid in order to ion exchange dissolved Cu ions with an excess of protons (Figure 1c).

Figure 2 demonstrates the measured voltammetric responses of a $Pt_{25}Cu_{75}$ precursor electrocatalyst during slow potential cycles between 0.05 and 1.2 V at 20 mV/s. The slow cycles were recorded to probe the state of the surface at various stages of the preparation of the active catalyst phase. The solid cyclic voltammogram (CV) in Figure 2 represents the very initial voltammetric response. The absence of the characteristic anodic stripping peaks associated with underpotentially deposited (upd) hydrogen on Pt surface atoms between 0.05 and 0.4 V indicates an almost pure Cu surface layer for the $Pt_{25}Cu_{75}$ alloys. This is in line with prediction of Cu surface segregation in Cu rich Pt−Cu alloys.[32] The anodic peaks at 0.3 and 0.7 V on the initial CV suggest selective Cu dissolution from the Cu rich $Pt_{25}Cu_{75}$ alloy precursor material. The anodic voltammetric feature at 0.9 V indicates the formation of Pt surface oxides. On the cathodic scan, reduction peaks at around 0.7 and 0.2 V are associated with partial re-reduction of Pt-oxides and re-deposition of Cu, while hydrogen evolution becomes the dominant faradaic process at potentials below 0.05 V. After a total of 200 cycles, the observed CV (dashed line in Figure 2) became time stable, indicating that Cu dissolution from the nanoparticle surface had either ceased or dropped to undetectable levels. The CV resembled that of a pure Pt nanoparticle catalyst[1,31] with the familiar H upd ad/desorption range (0.05−0.4 V/RHE) as well as the Pt (hydr)oxide formation and desorption peaks at 0.87 and 0.75 V on the anodic and cathodic scan, respectively. After dealloying the fuel cell was disassembled and the MEA was ion exchanged in 1 M H_2SO_4 for 2 h at 80 °C followed by thorough rinsing in deionized water. The fuel cell was then reassembled and another CV was measured. The dotted line in Figure 2 shows that the CV of the dealloyed cathode catalysts remained essentially identical after the ion exchange procedure.

TABLE 1: Catalyst Composition, Annealing Temperature, Dealloying Method, Electrochemical Surface Area, and Activities of Pt−Cu Bimetallic ORR Catalysts

catalyst comp. atom %	anneal. temp., °C	catalyst dealloying ethod	ECSA, m^2/g_{Pt}	mass activity @ 0.9V-IR free, A/mg_{Pt}	specific activity @ 0.9V-IR free, $\mu A/cm^2_{Pt}$
Pt_{100}[a]			63	0.104	166
$Pt_{80}Cu_{20}$	600		67	0.207	306
$Pt_{25}Cu_{75}$	600	chemical[b]	75	0.374	498
$Pt_{25}Cu_{75}$	600	electrochemical[c]	72	0.340	472
$Pt_{25}Cu_{75}$	800	electrochemical[c]	48	0.356	739
$Pt_{25}Cu_{75}$	950	electrochemical[c]	21	0.413	1964

[a] 45 wt % Pt loading on carbon support (Tanaka Kikinzoku International, Inc.). [b] Ex situ catalyst powder acid wash. [c] In situ MEA cathode layer voltammetry.

3.2. Electrocatalytic ORR Activity of Dealloyed Pt−Cu Nanoparticles in Single Fuel Cells. To establish relationships between the surface catalytic activity of dealloyed Pt−Cu nanoparticles for the electroreduction of oxygen in a single PEMFC and its synthesis and dealloying conditions, five distinct carbon-supported Pt−Cu alloy nanoparticles catalyst precursors were synthesized, dealloyed, tested and compared to a state-of-the-art Pt catalyst. The Pt weight loading of the carbon supported alloy precursor catalysts ranged from 22 to 27 wt %. Table 1 summarizes the synthesis, dealloying conditions and the MEA testing results of the catalysts. Three $Pt_{25}Cu_{75}$ precursors, annealed at 600, 800, and 950 °C, were electrochemically dealloyed using voltammetric cycling between 0.5 and 1.0 V as described in the previous paragraph (Figure 2). Furthermore, a $Pt_{25}Cu_{75}$, prepared at 600 °C, was chemically dealloyed using a washing procedure in hot 1 M H_2SO_4. The chemical and electrochemical dealloying procedures of $Pt_{25}Cu_{75}$ precursors typically resulted in a final catalyst composition of $\sim Pt_{80}Cu_{20}$ under the conditions chosen in this study. This is why the performances of the four dealloyed Pt−Cu catalysts were compared to a $Pt_{80}Cu_{20}$ precursor catalyst that was not subjected to Cu dealloying prior to fuel cell testing. The direct comparison of the dealloyed catalysts with the $Pt_{80}Cu_{20}$ alloy catalyst was to directly determine the activity benefits achieved after the dealloying activation process at comparable total catalyst composition. All alloy catalysts were compared against a 45 wt % commercial Pt catalyst (TKK Inc.) tested under identical conditions.

The measured PEMFC potential−current ($V-I$) polarization curves of the prepared catalysts are compared in Figure 3 (also see data in Table 1). The $V-I$ curves are mainly governed by the surface reaction kinetics up to geometric current densities of 0.2 A/cm^2. At larger current densities, ohmic resistance losses as well as mass transfer effects become significant. In Figure

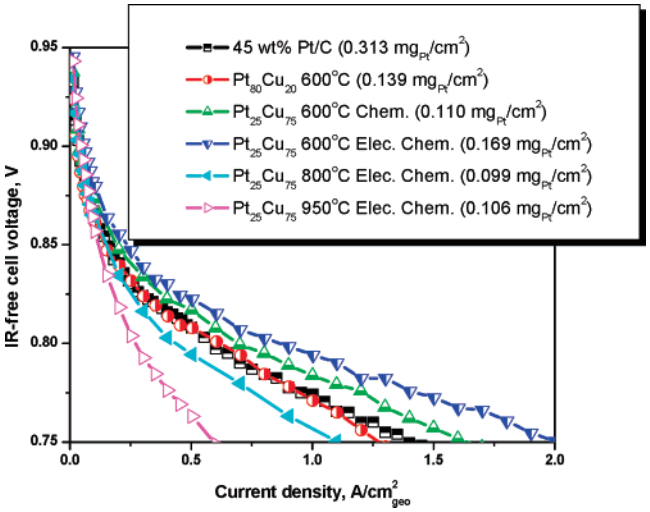

Figure 3. Current−voltage characteristics of chemically/electrochemically activated $Pt_{25}Cu_{75}$ precursors.

3, the linear current density scale in the kinetic region does not allow for a precise ranking of relative catalytic activity. It is apparent, however, that high temperature annealing (950 and 800 °C) has a detrimental effect on the mass transfer characteristics of the carbon-supported catalysts. This is likely attributable to a change in carbon surface functional groups leading to changes in interaction of the carbon support with water and/or ionomer during the catalyst ink and MEA preparation. Similar inferior mass transport characteristics have been observed in RDE test of the ORR activity of carbon supported Pt alloy catalysts after thermal annealing to 950 C.[9,10,31] The electrochemically and chemically dealloyed $Pt_{25}Cu_{75}$ catalysts annealed at 600 °C exhibited the most favorable $V-I$ characteristics over the entire current density range at a much reduced Pt loading of only 0.169 and 0.11 mg_{Pt}/cm^2 compared to the Pt standard catalyst with 0.313 mg_{Pt}/cm^2.

Figure 4 and Table 1 compare the kinetic Pt-mass activity (Figure 4a) for oxygen reduction as well as the intrinsic kinetic Pt-surface-area based activity (also referred to as specific activity[1]) (Figure 4b) of all catalysts. The logarithmic current density scale allows for an accurate relative activity ranking at 0.9 V cell voltage. Table 1 also reports the measured electrochemical surface areas (ECSA) of all catalysts. The ECSA value, the Pt mass-based and the specific activity (see Table 1) of the Pt standard, is very consistent with the reported state-of-the-art values.[1] The chemically and electrochemically dealloyed catalysts exhibited high, previously unachieved[1] Pt mass activity improvements of a factor of 3.5−4.1× compared to the standard Pt. The observed Pt specific activity was up to twelve times higher than that of the standard Pt. In situ electrochemically dealloyed $Pt_{25}Cu_{75}$, prepared at 950 °C, exhibited the highest Pt mass activity of 0.41 A/mg_{Pt} among the considered materials. It also showed a very high specific activity of 1964 $\mu A/cm^2$ at 0.9 V. The other two electrochemically dealloyed catalysts showed Pt mass based performances comparable to that of the chemically dealloyed material. As expected, the specific activity values strongly correlate inversely with the ECSA values. The activity of the as-prepared $Pt_{80}Cu_{20}$ catalyst exceeded that of Pt by a factor of 2, and is thus comparable to other Pt-rich $Pt_{1-x}M_x$ bimetallic catalyst systems for ORR, such as Pt−Co or Pt−Ni[9,10,13,22,28,33−35] when tested under comparable MEA conditions[1].

The results reported in Figure 4 and Table 1 display the significant activity advantage of dealloyed Cu-rich Pt−Cu

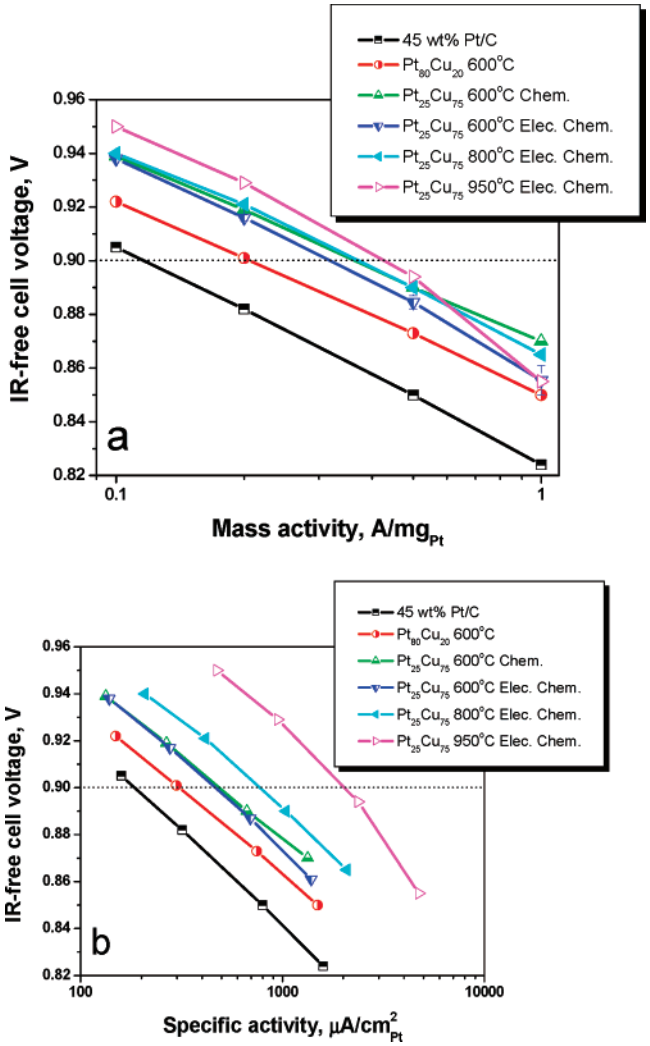

Figure 4. Catalytic oxygen reduction activities of Pt−Cu PEMFC cathode electrocatalysts. (a) Cell voltage (V) vs Pt mass activity (A/mg_{Pt}) (b) cell voltage (V) vs Pt surface area activity ($\mu A/cm^2_{Pt}$). Activity rankings are established at 0.9 V cell voltage (Table 1). Specific activity represents the intrinsic activity of a catalyst per unit Pt surface area. All cell potentials are corrected for ohmic losses.

electrocatalysts for ORR over conventional Pt-rich alloy catalysts and confirm previous RDE studies on dealloyed Pt−Cu catalysts for the electroreduction of oxygen in acidic media[32] where dealloyed carbon supported Pt−Cu nanoparticle catalysts were found to be 4−5 times more active than a state-of-the-art pure Pt nanoparticle electrocatalyst. While dealloying of Cu ions into a liquid electrolyte during RDE experiments did not affect the ORR measurements and therefore did not require a removal of Cu ions prior to activity tests, a Cu ion exchange step was crucial for MEA measurements. The favorable fuel cell activities also show that the novel three-step in situ dealloying preparation of the active catalyst phase (Figure 1) lends itself well to a realistic MEA configuration without compromising other MEA components, such as the membrane or the anode.

Figure 5 shows the cyclic voltammetric profile of the standard Pt and dealloyed Pt−Cu cathodes recorded at the end of the fuel cell MEA testing. The electrochemical surface areas (ECSA) obtained by integrating the H ad/desorption peaks are summarized in Table 1. Due to its high geometric Pt mass loading, the standard Pt catalyst showed the largest surface area in absolute, while with increasing annealing temperature the ECSA dropped significantly due to particle growth. The effect of alloy composition on surface area is reflected by comparing

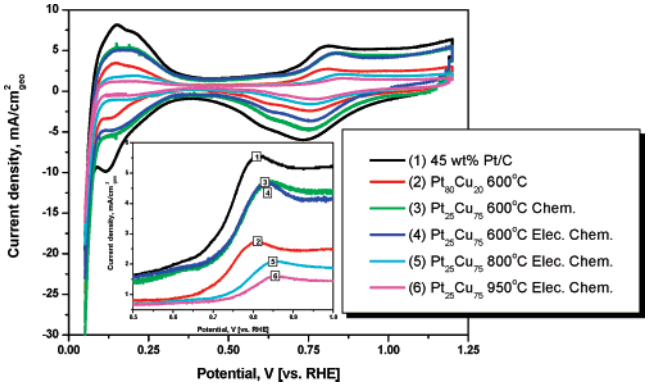

Figure 5. Cyclic voltammogram of the chemically/electrochemically activated catalysts. Position of the peak anodic current densities due to oxidation of surface atoms (coverage of hydroxide species) are marked with square symbol to show the positive shift in water activation potential of the catalysts in the inset.

the three Pt−Cu catalysts prepared at 600 C. Both the chemical and the electrochemically dealloyed samples showed a slightly increase surface area compared to the $Pt_{80}Cu_{20}$ material at comparable Pt mass loadings possibly indicating the effect of some surface roughening in the Cu depleted catalysts.

The inset of Figure 5 highlights the potential range where water activation leads to surface Pt−OH formation according to $Pt + H_2O \rightarrow Pt{-}OH + H^+ + e^-$. Anodic shift of the peak potentials for the dealloyed catalysts compared to pure Pt or the $Pt_{80}Cu_{20}$ catalyst suggested a delayed formation of Pt−OH surface species during anodic sweeps. A shift of the Pt−OH onset potential was frequently observed before for Pt alloy electrocatalysts and was either considered the cause for enhanced ORR activity[25,27,36] or was perceived more of an effect of a reduced Pt−O chemisorption energy.[24,26,37]

3.3. Origin of the Activity Enhancement and the Role of Surface Roughening. The ECSA values reported in Table 1 reflect that the origin of the significant ORR activity improvements is unlikely to be a surface-roughening based mechanism.[38,39] Whereas dealloying of bimetallic alloy interfaces has been reported to roughen the electrochemical interface and result in increased surface areas,[40] the data in Table 1 shows that the ECSA values of the dealloyed catalysts prepared at 800 and 950 C are actually lower than that of the standard Pt catalyst. Even though the ECSA values of the materials prepared at 600 °C are slightly higher than that of the standard Pt value, they cannot account for the 3−4 fold activity increases, because activity is expected to scale linearly with ECSA. It should also be noted that the ECSA values of all the Pt−Cu alloy electrocatalysts in Table 2 were consistently lower than that of the 30 wt % carbon-supported Pt catalyst (82 m^2/g_{Pt}) which was used as starting material for the alloy synthesis. The electrochemical Pt surface area decreased during the synthesis and annealing process and even after de-alloying did not come back to the surface area values of the starting material.

With surface roughening ruled out as the origin for the activity enhancements, geometric (surface structure) effects and/or electronic (ligand) effects[37,41−48] become likely candidates to explain the modified surface catalytic activity. Both geometric and ligand effects can be caused by the surface atomic environment of distinct metal atoms which modify their electronic structure, and hence, their chemisorption and catalytic properties.

3.4. Relation between Compositional Stability and the Dealloying Method. To gain insight into the stability of the active phases of the dealloyed Pt−Cu catalysts, their surface and bulk compositions were measured using ICP/EDX and XPS after synthesis, after dealloying, and after MEA testing. The objective was a comparative evaluation of chemical versus the electrochemical dealloying with respect to their effectiveness to yield stable and active catalyst phases. Figures 6 and 7 report the detailed XPS spectra of the dealloyed catalysts from which the near surface composition of the alloy particles in Table 2 were estimated (estimated probing depth 5 atomic layers). Table 2 also reports the ICP/EDX bulk compositions.

TABLE 2: Bulk and Surface Compositions of the Dealloyed Pt−Cu Bimetallic Catalysts

catalyst comp. atom %	anneal. temp., °C	catalyst dealloying method	bulk comp. (ICP/EDX), atom %	near surface comp. (XPS), at %
$Pt_{80}Cu_{20}$	600		$Pt_{78}Cu_{22}$[c,e]	$Pt_{50}Cu_{50}$[e]
$Pt_{25}Cu_{75}$	600	chemical[a]	$Pt_{60}Cu_{40}$[c,f]	$Pt_{28}Cu_{72}$;[e] $Pt_{81}Cu_{19}$;[f] $Pt_{90}Cu_{10}$[h]
$Pt_{25}Cu_{75}$	600	electrochemical[b]	$Pt_{87}Cu_{13}$[c,g]	$Pt_{28}Cu_{72}$;[e] $Pt_{98}Cu_2$[g]
$Pt_{25}Cu_{75}$	800	electrochemical[b]	$Pt_{82}Cu_{18}$[d,g]	$Pt_{92}Cu_8$[g]
$P_{25}Cu_{75}$	950	electrochemical[b]	$Pt_{61}Cu_{39}$[d,g]	$Pt_{88}Cu_{12}$[g]

[a] Ex situ catalyst powder acid wash. [b] In situ MEA cathode layer voltammetry. [c] ICP analysis. [d] EDX analysis. [e] As prepared. [f] After chemical dealloying and before fuel cell testing. [g] After electrochemical dealloying and fuel cell testing. [h] After chemical dealloying and after fuel cell testing.

Near Surface Compositions. Figure 6a,b shows the Pt4fand $Cu2p_{3/2}$ spectra of the dealloyed Pt−Cu bimetallic catalysts. Peak binding energies revealed the presence of mostly metallic Pt 71.3 eV,[49] possibly contaminated with some PtO 74.6 eV[49] and PtO_2 74.9 eV[49] species (not deconvoluted in Figure 6). In contrast to the precursor materials, much reduced amounts of metallic Cu (932.8 eV[49]) were detected in the chemically dealloyed samples, while only trace amounts of metallic Cu remained near the surface in case of the electrochemically dealloyed catalysts (Table 2). No significant amounts of CuO species were observed in the dealloyed catalyst which indicates that only few, if any, Cu atoms are present in the first layer, as these atoms would very likely form Cu (hydr)oxide species upon contact with acidic liquid electrolytes.[50] This is in agreement with the observed cyclic voltammetric profiles that indicated no detectable amount of residual Cu atoms in the surface. The XPS data give evidence that the near-surface region of the dealloyed Pt−Cu catalysts was severely enriched in Pt compared to the precursor materials.

Chemical versus Electrochemical Dealloying. The compositional data of the two dealloyed $Pt_{25}Cu_{75}$ precursors, annealed at 600 °C, (Table 2) suggests that electrochemical (cyclic voltammetric) dealloying results in a more complete Cu dissolution than chemical acid leaching. The surface atomic composition of the chemically dealloyed (acid washed) $Pt_{25}Cu_{75}$ precursor (600 C) after dealloying and before ORR testing was $Pt_{81}Cu_{19}$, and therefore was Cu richer compared to the $Pt_{93}Cu_7$ composition measured for an electrochemically dealloyed (cyclic voltammetry) 600 C $Pt_{25}Cu_{75}$ precursor before ORR testing.[31] After catalytic testing, the chemically dealloyed catalyst showed a surface composition of $Pt_{90}Cu_{10}$, while the corresponding electrochemically dealloyed material resulted in a final near surface composition of $Pt_{98}Cu_2$ after measuring MEA polarization curves. Figure 7a,b shows the corresponding detailed Photoemission spectra of the chemically dealloyed $Pt_{25}Cu_{75}$ 600 C material in the Pt4f and Cu2p regions: The photoemission peak at the $Cu2p_{3/2}$ binding energy before recording the MEA polarization curves (Figure 7b, top) is

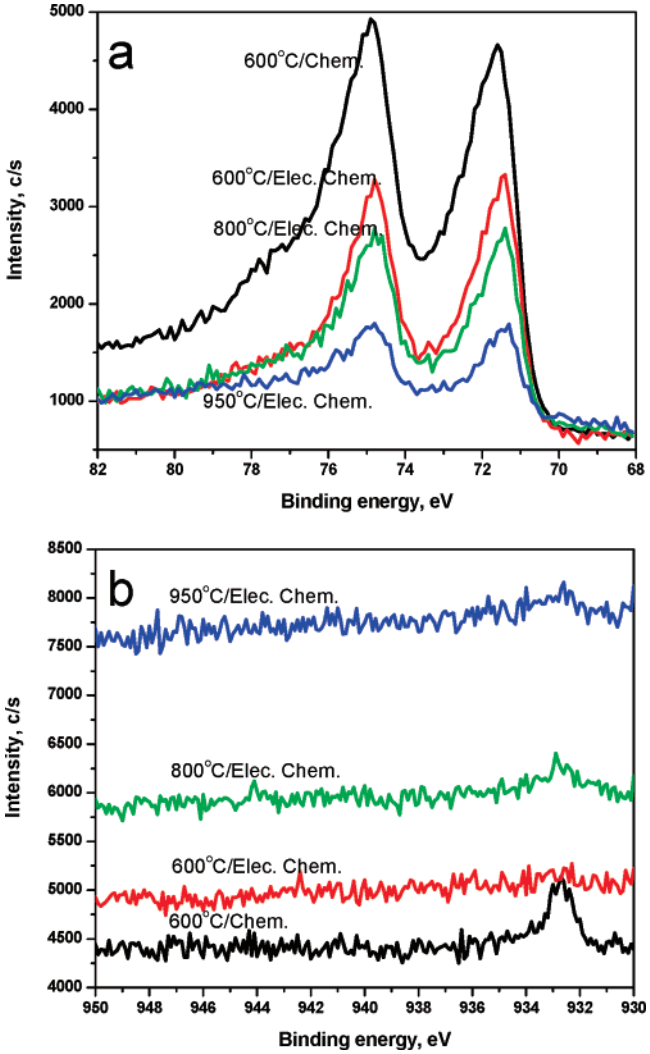

Figure 6. X-ray photoelectron emission spectra of (a) Pt4f and (b) Cu2p core level regions of the four chemically and electrochemically dealloyed $Pt_{25}Cu_{75}$ precursors reported in Table 1. Labels indicate annealing conditions and dealloying method. Peak area integration resulted in the Pt:Cu near surface ratios provided in Table 2. The chemically dealloyed sample was measured before fuel cell testing, the others after.

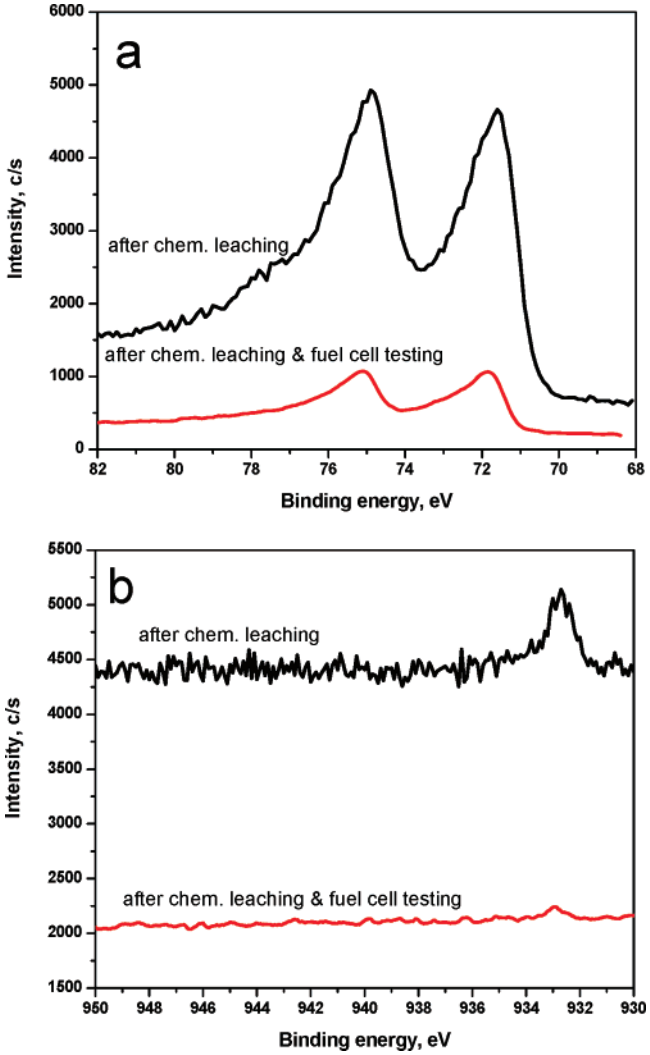

Figure 7. X-ray photoelectron emission spectra of (a) Pt4f and (b) Cu2p core level region of the chemically leached Pt−Cu cathode catalyst powder before and after fuel cell testing. Additional Cu dissolution occurred for the acid leached catalyst during MEA testing. Peak area integration resulted in Pt:Cu atomic ratios reported in Table 2.

severely reduced compared to that after fuel cell testing (Figure 7b, bottom) due to additional Cu leaching from the cathode layer during MEA operation. For both chemical and electrochemical dealloying, additional Cu atoms seemed to dissolve during the MEA performance testing, although, the MEA was not exposed to more positive potentials during testing than those applied during dealloying.

The surface compositional changes after MEA testing suggest that both chemical and electrochemical Cu dealloying procedures did not result in a thermodynamically and therefore compositionally stable active catalyst phase. The dealloying processes in both cases were likely limited by Cu atomic transport to the surface. Additional Cu leaching from the catalyst surface during MEA operation is likely to have a detrimental long-term effect on the ohmic resistance and, therefore, the performance of a MEA. Hence, to keep additional leaching to a minimum, the cyclic voltammetric dealloying method, appears as the preferable dealloying method under the present conditions.

To rationalize the differences in the extent of dealloying between acid wash and cyclic voltammetric treatment it is helpful to recall that chemical treatment of Pt−Cu alloys in air-saturated acids represents an electroless dissolution process at an open circuit (mixed) potential with the open circuit potential governed by all redox systems (metal and surface reactions) present. Chemical dealloying of Pt−Cu alloys in air saturated acid occurs at a constant potential that ranges between that of the Cu standard potential (0.34 V/NHE) and the open circuit potential of a pure Pt cathode catalyst in a hydrogen/air fuel cell (typically around 0.95−1 V RHE). Since the potential is constant, passivation processes can build up protective surface layers which inhibit bulk dealloying or slow down diffusion of Cu atoms to the surface[51−54]. In contrast, the controlled cyclic voltammetric potential sweeps between 0.5 and 1.0 V/RHE (voltammetric dealloying) entails repeated cycles of surface atomic oxidation/dissolution followed by Pt-oxide re-reduction. These processes are likely combined with a larger extent of potential-induced surface atomic rearrangements which expose subsurface atomic layers and lead to a more complete Cu dissolution.[51−56]

Bulk Compositions. A similar trend in the composition and degree of leaching between chemical and electrochemical dealloying was obvious from the EDX bulk compositional analyses of the 600 C precursor materials given in Table 2. A previous study reported that electrochemical dealloying of a $Pt_{25}Cu_{75}$ precursor (annealed at 600 C) resulted in a bulk composi-

tion of $Pt_{79}Cu_{21}$[31] before testing, and in $Pt_{87}Cu_{13}$ after MEA testing (Table 2). In contrast, chemical dealloying resulted in a $Pt_{60}Cu_{40}$ composition before MEA testing.

Generally, it is unclear whether Cu surface dealloying from Pt−Cu bimetallics can result in a Cu depleted alloy which is thermodynamically stable under fuel cell operating conditions. The present findings do not preclude the existence of a thermodynamically stable Cu-depleted catalyst structure. Advanced density functional theory (DFT) calculations of metal dissolution processes may help predict a thermodynamically stable dealloyed Pt−Cu particle structure.[32,47,50] The addition of a third element in the precursor may also help stabilize the dealloyed nanoparticle structure and composition. If a thermodynamically stable composition does not exist or is not attainable by dissolution processes, the dealloying process continues to be controlled by Cu atom transport (most likely Cu bulk diffusion) and would eventually terminate in the complete removal of all Cu atoms from the nanoparticle precursors. In this case the active catalyst phase would be transient in nature. However, from a practical fuel cell device point of view, a diffusion-controlled dealloying process is acceptable, if the time scale of Cu dissolution reaches those of the device lifetime. In the case of a diffusion-controlled Cu dissolution process, the dealloying protocol which removes the most Cu from the surface at comparable performances would be the preferred one.

3.5. Alloy Phase Structure Analysis. X-ray diffraction patterns of the $Pt_{25}Cu_{75}$ precursors materials prepared at the three annealing temperatures are compared in Figure 8a. All materials crystallized in a similar disordered face-centered-cubic (fcc) structure, with the (111) fundamental reflection occurring in a 2θ range from 41.8° to 43° depending on the detailed alloy phase composition. For Pt−Cu bimetallics, Vegard's law provides an excellent mapping between phase composition and unit cell parameters. At 600 °C, sharp Cu reflections indicate the presence of an unalloyed pure Cu phase. With increasing annealing temperatures, the alloy uniformity improved significantly. Reduced peak widths and an upshift of the (111) reflection to $2\theta = 42°$ suggest temperature induced growth of well alloyed Pt−Cu crystallites. Even at 950 °C, despite a generally uniform Pt−Cu alloy phase structure, peak shoulders indicate the presence of a bit of unalloyed Cu. Figure 8b demonstrates how chemical dealloying affects the phase structure of a $Pt_{25}Cu_{75}$ 600 C precursor catalyst. The bottom profile reports the annealed precursor patterns prior to dealloying. The center profile shows the acid washed catalyst and evidence how the dealloying procedure removes the unalloyed Cu phase. Furthermore, the Pt−Cu (111) reflection shifts from 41.8° to 41° suggesting a partial dissolution of Cu from the initial Pt−Cu alloy phase. Comparison to the pure Pt(111) peak position (39.7°) indicates that residual Cu (~40 atomic %, ICP) remained in the chemically dealloyed material. The top profile in Figure 6b represents the structure of the as-prepared $Pt_{80}Cu_{20}$ catalyst. Absence of Cu peaks suggests uniform alloying. The alloy (111) reflection (40.5°) is consistent with its composition according to Vegard's law. In a similar previous RDE study[31] of voltammetrically dealloyed $Pt_{25}Cu_{75}$ ORR catalysts, the catalyst annealed at 800 °C performed superior to that annealed at 950 °C in terms of Pt mass and specific activity after a similar dealloying procedure. To explain the discrepancy to the present study, a comparison of the XRD profiles provided clues: In the previous study, the 800 °C annealed catalysts exhibited a XRD peak pattern and intensity ratio between Pt−Cu alloy phase and pure Cu phase similar to that of the present 950 °C sample. This observation raises the issue whether a rough evaluation of the ORR activity of dealloyed $Pt_{25}Cu_{75}$ catalyst could be possible based on an XRD pattern alone.

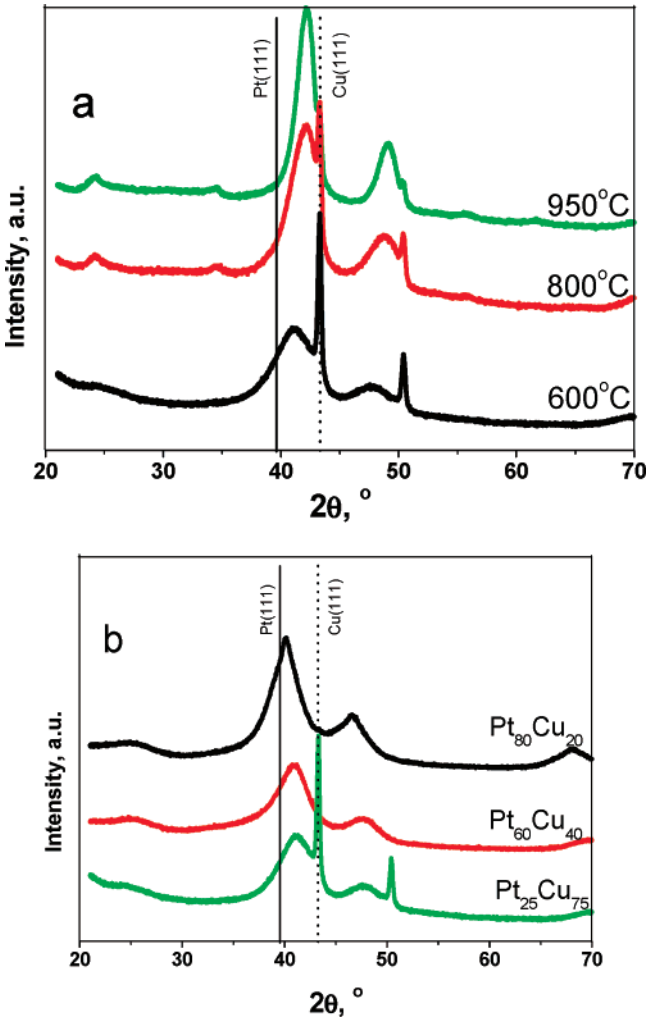

Figure 8. (a) X-ray diffraction profiles of carbon-supported $Pt_{25}Cu_{75}$ precursor catalysts annealed at 600, 800, and 950 °C. All materials show disordered face-centered-cubic (fcc) symmetry. High temperatures (800 and 950 °C) induced slight graphitization of the carbon black support seen by peaks at 24° and 34°. (b) X-ray diffraction profile of the carbon-supported $Pt_{80}Cu_{20}$ cathode catalyst (top), of the chemically dealloyed $Pt_{25}Cu_{75}$ precursor catalyst (resulting in a composition $Pt_{60}Cu_{40}$, center), and of the as-prepared $Pt_{25}Cu_{75}$ (600 °C) precursor (bottom).

3.6. Impact of Alloy Uniformity on Compositional Stability and Extent of Dealloying. In this section, the impact of the annealing temperature of the $Pt_{25}Cu_{75}$ precursors on the extent of voltammetric dealloying will be investigated using the compositional data in Table 2. The present data suggest that the amount of Cu removed from the precursor is strongly correlated with the annealing temperature. The higher the annealing temperature, the higher was the Cu bulk and surface concentration retained in the dealloyed catalyst particles after MEA testing: For example, the 950 C catalyst showed a Cu content of 39 and 12 at % in the bulk and in the surface after MEA testing, respectively (Table 2) which was significantly more Cu than in the 600 °C sample. Unless the dealloyed 950 °C catalyst composition is thermodynamically stable, its relatively high residual Cu content makes detrimental Cu dissolution under continued MEA operation likely. In fact, it is this catalyst which exhibited the least favorable polarization characteristics with increased ohmic and mass transport losses in Figure 3. This is consistent with the notion that the 950 °C

catalyst lost the least amount of Cu during the dealloying protocol and continues to dissolve Cu ions into the membrane during MEA testing. Interestingly, however, the 950 °C catalyst exhibited the highest kinetic Pt mass based and specific electrocatalytic activity which bears the question whether a somewhat Cu richer bulk (∼40 atom %) and surface (∼12 atom %) composition may be actually favorable for the surface catalysis. If so, the 800 and 600 °C catalyst may have passed through a similar active compositional state during the dealloying protocol, yet since their Cu dealloying rate was higher, the Cu composition at the time of MEA testing was already below the optimum. This discussion highlights the trade-offs between activity and stability of Pt alloy nanoparticles and demonstrates the difficulties one faces with a clear evaluation of relative alloy stability. Only long-term tests will ultimately be able to tell whether the compositional stability of a given ORR catalyst will be sufficient for practical durable cathodes.

3.7. Structural Model for Dealloyed Pt−Cu Bimetallic Nanoparticles. A consistent structural and compositional model for the dealloyed Pt−Cu nanoparticles emerges combining the XRD structural and compositional as well as the EDX and XPS compositional data. During the dealloying process, Cu atoms rapidly dissolve from the surface of the Cu rich precursor particles. With increasing removal of Cu atoms from the top layer, Cu atoms start to move from the particle core toward the particle surface. Considering a slow Cu bulk movement compared to a fast surface Cu dissolution, the particle surface eventually depletes to relatively low concentrations of Cu after dealloying. The catalyst particle cores still contain substantial amounts of Cu atoms (up to at least 13−40 at %) and a compositional gradient is established across the alloy particles. Hence, the active dealloyed Pt−Cu catalysts can be represented by a Pt enriched surface region (particle shell) surrounding an increasingly Cu-richer particle core. A hypothetical structural model of the dealloyed catalysts is depicted in Figure 1c and has been referred to as a dealloyed Pt−Cu core−shell nanoparticle catalyst.[31,57] Being Cu rich, the core of the dealloyed particles exhibits a reduced lattice parameters compared to pure Pt (see Figure 8). We hypothesize that the reduced lattice parameters in the core may affect the Pt interatomic distance of the Pt rich surface giving rise to somewhat reduced Pt−Pt distances. This mechanism has been previously shown to result in modified surface catalytic activity.[58−61]

4. Conclusion

We have presented a new class of highly efficient Pt−Cu alloy nanoparticle electrocatalysts for the electroreduction of oxygen at PEMFC cathodes. The active phase of the Pt−Cu alloy nanoparticle electrocatalysts were prepared by Cu dealloying, that is selective dissolution of Cu atoms from the nanoparticle surface, of a $Pt_{25}Cu_{75}$ alloy precursor compound. The dealloyed Pt−Cu catalysts showed a surface catalytic improvement of a factor of up to 4 in terms of Pt mass activity[1] and of more than 10x in terms of specific activity compared to a state-of-art Pt cathode catalyst.[1]

We have demonstrated the viability of an in-situ voltammetric dealloying procedure inside the cathode layer followed by an ion exchange step of excess Cu ions in order to prepare the active catalyst phase inside the MEA. This catalyst activation procedure by dealloying was shown to lend itself well to the conventional MEA structure of PEMFCs and therefore does not require any significant modification of the state-of-the-art technology.

Chemical dealloying procedures (acid washes) were compared against voltammetric dealloying procedures. At given synthesis conditions, electrochemical dealloying methods were more effective in the removal of Cu from the precursor compounds compared to voltammetric dealloying procedures minimizing Cu ion contaminations after ion exchange.

The extent of Cu removal by voltammetric methods depended significantly on the annealing temperature of the precursor alloy. Uniformly alloyed Pt−Cu nanoparticles prepared at 950 °C lost less Cu at a given dealloying protocol and exhibited the most favorable ORR Pt mass and specific activities despite their low surface areas. This underlined the fine balance between alloy catalyst stability and ORR activity.

Surface area measurements after dealloying have ruled out a surface roughening mechanism as the origin for the observed ORR activity enhancements in favor of electronic and/or geometric surface effects. Compositional analysis points to a Cu-rich core- Pt-enriched shell structure as a model for the dealloyed particles. The sharply lattice-contracted core region may result in a reduced Pt−Pt interatomic distance in the Pt rich surface region in line with early theoretical predictions on the effect of geometric atomic arrangements on catalytic surface rates.[60−62]

Future studies must focus on the molecular processes associated with voltammetric dealloying of base metal rich bimetallic alloy nanoparticle precursors. More detailed structural studies are needed to clarify the structural state of the Pt enriched particle shells. For this purpose, direct space methods ((S)TEM) and reciprocal space techniques (small-angle X-ray scattering) need to be utilized to test the core−shell hypothesis. Current activities also focus on the question whether Pt−Cu core−shell structures with similar characteristics can be fabricated by electro- or vapor deposition techniques. Finally, from a more practical device point of view, the impact of the dealloying procedure on the structure of the membrane-electrode-assembly at the meso- and macro scale (swelling, rupture, deformation, residual metal ion concentration in membrane, and anode) has to be investigated in more detail.

Beyond its use in the electroreduction of oxygen (ORR), the presented class of preferentially dealloyed catalysts also provides a more general strategy toward the deliberate modification of surface catalytic properties of other noble metals, e.g., of Pd, Ru, or Rh. Starting from Cu-rich, or, more generally, from base-metal-rich precursor compounds, the obtained lattice structure modification of the noble-metal-rich particle shells may result in a modified binding of surface reaction intermediates, and so offer deliberate control over the surface catalytic reactivity of noble metal surfaces.

Acknowledgment. This project was supported by the Department of Energy, Office of Basic Energy Sciences (BES), under Grant LAB04-20 via a subcontract with Stanford Synchrotron Radiation Laboratory, and by the National Science Foundation, Award No. 0729722. Acknowledgment is made to the Donors of the American Chemical Society Petroleum Research Fund for partial support of this research (Grant No. 44165). We also acknowledge financial support by the Houston Area Research Center (HARC) under the NanoEnergy Collaborative.

References and Notes

(1) Gasteiger, H. A.; Kocha, S. S.; Sompalli, B.; Wagner, F. T. *Appl. Catal. B: Environ.* **2005**, *56*, 9−35.

(2) Li, X. *Principles of Fuel Cells*; Taylor−Francis: New York, 2006.

(3) O'hayre, R.; Cha, S.-W.; Colella, W.; Prinz, F. B. *Fuel Cell Fundamentals*; Wiley: New York, 2006.

(4) Steele, B. C. H.; Heinzel, A. *Nature* **2001**, *414*, 345−352.

(5) Luczak, F. J.; Landsman, D. A. *Ternary fuel cell catalysts containing platinum, cobalt and chromium.* US Patent No. 4,447,506, 1984.

(6) Beard, B. C. J. Philip N. Ross, *J. Electrochem. Soc.* **1990**, *137*, 3368−3374.
(7) Mukerjee, S.; Srinivasan, S. *J. Electroanal. Chem.* **1993**, *357*, 201−224.
(8) Min, M.-K.; Cho, J.; Cho, K.; Kim, H. *Electrochim. Acta* **2000**, *45*, 4211−4217.
(9) Koh, S.; Toney, M. F.; Strasser, P. *Electrochim. Acta* **2007**, *52*, 2765−2774.
(10) Koh, S.; Leisch, J.; Toney, M. F.; Strasser, P. *J. Phys. Chem. C* **2007**, *111*, 3744−3752.
(11) Jalan, V.; Taylor, E. J. *J. Electrochem. Soc.* **1983**, *130*, 2299−2302.
(12) Xu, H.; Kunz, H. R.; Bonville, L. J.; Fenton, J. M. *J. Electrochem. Soc.* **2007**, *154*, B271−B278.
(13) Koh, S.; Yu, C.; Mani, P.; Srivastava, R.; Strasser, P. *J. Power Source* **2007**, *172*, 50−56.
(14) Lima, F. H. B.; Lizcano-Valbuena, W. H.; Teixeira-Neto, E.; Nart, F. C.; Gonzalez, E. R.; Ticianelli, E. A. *Electrochim. Acta*, **2006**, *52*, 385−393.
(15) Wakabayashi, N.; Takeichi, M.; Uchida, H.; Watanabe, M. *J. Phys. Chem. B* **2005**, *109*, 5836−5841.
(16) Pharkya, P.; Alfantazi, A.; Farhat, Z. *J. Fuel Cell Sci. Technol.* **2005**, *2*, 171−178.
(17) Zeng, J.; Lee, J. Y. *J. Power Sources* **2005**, *140*, 268−273.
(18) Antolini, E.; Salgado, J. R. C.; Giz, M. J.; Gonzalez, E. R. *Int. J. Hydrogen Energy* **2005**, *30*, 1213−1220.
(19) Salgado, J. R. C.; Antolini, E.; Gonzalez, E. R. *Appl. Catal. B* **2005**, *57*, 283−290.
(20) Salgado, J. R. C.; Antolini, E.; Gonzalez, E. R. *J. Phys. Chem. B* **2004**, *108*, 17767−17774.
(21) Salgado, J. R. C.; Antolini, E.; Gonzalez, E. R. *J. Power Sources* **2004**, *138*, 56−60.
(22) Paulus, U. A.; Wokaun, A.; Scherer, G. G.; Schmidt, T. J.; Stamenkovic, V.; Radmilovic, V.; Markovic, N. M.; Ross, P. N. *J. Phys. Chem. B* **2002**, *106*, 4181−4191.
(23) Xiong, L.; Manthiram, A. *J. Electrochem. Soc.* **2005**, *152*, A697−A703.
(24) Norskov, J. K.; Rossmeisl, J.; Logadottir, A.; Lindqvist, L.; Kitchin, J. R.; Bligaard, T.; Jonsson, H. *J. Phys. Chem. B* **2004**, *108*, 17886−17892.
(25) Stamenkovic, V.; Mun, B. S.; Arenz, M.; Mayerhofer, K. J. J.; Lucas, C. A.; Wang, G.; Ross, P. N.; Markovic, N. *Nat. Mater.* **2007**, *6*, 241.
(26) Stamenkovic, V.; Moon, B. S.; Mayerhofer, K. J.; Ross, P. N.; Markovic, N.; Rossmeisl, J.; Greeley, J.; Norskov, J. K. *Angew. Chem., Int. Ed.* **2006**, *45*, 2897−2901.
(27) Stamenkovic, V. R.; Fowler, B.; Mun, B. S.; Wang, G.; Ross, P. N.; Lucas, C. A.; Markovic, N. M. *Science* **2007**, *315*, 493.
(28) Thompsett, D. In *Handbook of Fuel Cells - Fundamentals, Technology and Applications*; Vielstich, W.; Lamm, A.; Gasteiger, H. A., Eds.; Wiley: New York, 2003; Vol. 3, Chapter 437, p 467.
(29) Bashyam, R.; Zelenay, P. *Nature* **2006**, *443*, 63−66.
(30) Vukmiovic, M. B.; Zhang, J.; Sasaki, K.; Nilekar, A. U.; Uribe, F.; Mavrikakis, M.; Adzic, R. R. *Electrochim. Acta* **2007**, *52*, 2257−2263.
(31) Koh, S.; Strasser, P. *J. Am. Chem. Soc.* **2007**, *129*, 12624.
(32) Ruban, A. V.; Skriver, H. L.; Nørskov, J. K. *Phys. Rev. B* **1999**, *59*, 15990−16000.
(33) Mukerjee, S.; Srinivasan, S. *J. Electroanal. Chem.* **1993**, *357*, 201.
(34) Paulus, U. A.; Wokaun, A.; Scherer, G. G.; Schmidt, T. J.; Stamenkovic, V.; Markovic, N. M.; Ross, P. N. *Electrochim. Acta* **2002**, *47*, 3787−3798.
(35) Stamenkovic, V.; Schmidt, T. J.; Ross, P. N.; Markovic, N. M. *J. Phys. Chem. B* **2002**, *106*, 11970−11979.
(36) Markovic, N. M.; Ross, P. N. *Surf. Sci. Rep.* **2002**, *45*, 117.
(37) Greeley, J.; Norskov, J. K. *Surf. Sci.* **2005**, *592*, 104−111.
(38) Kim, K. T.; Kim, T. G.; Chung, J. S. *J. Electrochem. Soc.* **1995**, *142*, 1531−1539.
(39) Paffet, M. T.; Beery, J. G.; Gottesfeld, S. *J. Electrochem. Soc.* **1988**, *135*, 1431−1436.
(40) Erlebacher, J.; Aziz, M. J.; Karma, A.; Dimitrov, N.; Sieradzki, K. *Nature* **2001**, *410*, 450−453.
(41) Nilsson, A.; Pettersson, L. G. M.; Hammer, B.; Bligaard, T.; Christensen, C. H.; Norskov, J. K. *Catal. Lett.* **2005**, *100*, 111.
(42) Strasser, P.; Fan, Q.; Devenney, M.; Weinberg, W. H.; Liu, P.; Norskov, J. K. *J. Phys. Chem. B* **2003**, *107*, 11013.
(43) Greeley, J.; Norskov, J. K.; Mavrikakis, M. *Annu. Rev. Phys. Chem.* **2002**, *53*, 319−348.
(44) Nørskov, J. K.; Bligaard, T.; Logadottir, A.; Bahn, S.; Hansen, L. B.; Bollinger, M.; Bengaard, H.; Hammer, B.; Sljivancanin, Z.; Mavrikakis, M.; Xu, Y.; Dahl, S.; Jacobsen, C. J. H. *J. Catal.* **2002**, *209*, 275.
(45) Hammer, B.; Nørskov, J. K. *Adv. Catal.* **2000**, *45*, 71−129.
(46) Hammer, B.; Nørskov, J. K. In *Chemisorption and Reactivity on Supported Clusters and Thin Films*; Lambert, R. M., Pacchioni, G., Eds.; Kluwer Academic Publishers: The Netherlands, 1997; pp 285−351.
(47) Ruban, A.; Hammer, B.; Stoltze, P.; Skriver, H. L.; Nørskov, J. K. *J. Mol. Catal. A: Chem.* **1997**, *115*, 421.
(48) Hammer, B.; Nørskov, J. K. *Surf. Sci.* **1995**, *343*, 211−220.
(49) Wagner, C. D.; Naumkin, A. V.; Kraut-Vass, A.; Allison, J. W.; Powell, C. J.; Rumble, J. R. NIST X-ray Photoelectron Spectroscopy Database, Reference Database 20, version 3.4; NIST, Gathersburg, MD, 2003; http://srdata.nist.gov/xps/.
(50) Greeley, J.; Nørskov, J. K. *Electrochim. Acta* **2007**, *52*, 5829−5836.
(51) Corcoran, S. G. In *Critical Factors in Localized Corrosion III*; Kelley, R. G., Frankel, G. S., Natishan, P. M., Newman, R. C., Eds.; Electrochemical Society: Pennington, NJ, 2000; Vol. 98−17, pp 500−507.
(52) Davis, J. R. *Corrosion−Understanding the basics*; ASM International: Materials Park, OH, 2000.
(53) Williams, D. E.; Newman, R. C.; Song, Q.; Kelly, R. G. *Nature* **1991**, *350*, 216−219.
(54) Sieradzki, K.; Corderman, R. R.; Shukla, K.; Newman, R. C. *Philos. Mag. A* **1989**, *59*, 713−746.
(55) Pickering, H. W. *Corros. Sci.* **1983**, *23*, 1107−1120.
(56) Forty, A. J. *Nature* **1979**, *282*, 597−598.
(57) Srivastava, R.; Mani, P.; Hahn, N.; Strasser, P. *Angew. Chem. Int. Ed.* **2007**, *46*, 8988−8991.
(58) Lars, G.; Ye, X.; Manos, M. *Phys. Chem. Chem. Phys.* **2006**, *8*, 3369−3374.
(59) Zhang, J.; Vukmiovic, M. B.; Xu, Y.; Mavrikakis, M.; Adzic, R. R. *Angew. Chem., Int. Ed.* **2005**, *44*, 2132.
(60) Greeley, J.; Krekelberg, W. P.; Mavrikakis, M. *Angew. Chem., Int. Ed.* **2004**, *43*, 4296−4300.
(61) Mavrikakis, M.; Hammer, B.; Norskov, J. K. *Phys. Rev. Lett.* **1998**, *81*, 2819−2822.
(62) Xu, Y.; Mavrikakis, M. *Surf. Sci.* **2001**, *494*, 131.